Monthly Notices of the ROYAL ASTRONOMICAL SOCIETY

MNRAS **513,** 1785–1793 (2022) https://doi.org/10.1093/mnras/stac798
Advance Access publication 2022 March 29

TIC-320687387 B: a long-period eclipsing M-dwarf close to the hydrogen burning limit

Samuel Gill,[1,2]★ Solène Ulmer-Moll,[3] Peter J. Wheatley ,[1,2] Daniel Bayliss ,[1,2] Matthew R. Burleigh,[4] Jack S. Acton,[4] Sarah L. Casewell ,[4] Christopher A. Watson,[5] Monika Lendl ,[3] Hannah L. Worters,[6] Ramotholo R. Sefako,[6] David R. Anderson ,[1,2] Douglas R. Alves ,[7] François Bouchy,[3] Edward M. Bryant ,[1,2] Philipp Eigmüller,[8] Edward Gillen ,[9,10]† Michael R. Goad,[4] Nolan Grieves,[3] Maximilian N. Günther ,[11]‡ Beth A. Henderson,[4] James S. Jenkins ,[6,12] Lokesh Mishra,[3] Maximiliano Moyano ,[13] Hugh P. Osborn ,[14,15] Rosanna H. Tilbrook,[4] Stéphane Udry,[3] Jose I. Vines[7] and Richard G. West [1,2]

[1]*Department of Physics, University of Warwick, Gibbet Hill Road, Coventry CV4 7AL, UK*
[2]*Centre for Exoplanets and Habitability, University of Warwick, Gibbet Hill Road, Coventry CV4 7AL, UK*
[3]*Observatoire de Genève, Université de Genève, Chemin Pegasi 51, CH-1290 Sauverny, Switzerland*
[4]*School of Physics and Astronomy, University of Leicester, Leicester LE1 7RH, UK*
[5]*Astrophysics Research Centre, School of Mathematics and Physics, Queen's University Belfast, Belfast BT7 1NN, UK*
[6]*South African Astronomical Observatory, PO Box 9, Observatory 7935, Cape Town, South Africa*
[7]*Departamento de Astronomía, Universidad de Chile, Santiago, Chile*
[8]*Institute of Planetary Research, German Aerospace Center, Rutherfordstrasse 2., D-12489 Berlin, Germany*
[9]*Astronomy Unit, Queen Mary University of London, Mile End Road, London E1 4NS, UK*
[10]*Astrophysics Group, Cavendish Laboratory, J.J. Thomson Avenue, Cambridge CB3 0HE, UK*
[11]*European Space Agency (ESA), European Space Research and Technology Centre (ESTEC), Keplerlaan 1, NL-2201 AZ Noordwijk, the Netherlands*
[12]*Núcleo de Astronomía, Facultad de Ingeniería y Ciencias, Universidad Diego Portales, Av. Ejército 441, Santiago, Chile*
[13]*Instituto de Astronomía, Universidad Católica del Norte, Angamos 0610, 1270709 Antofagasta, Chile*
[14]*NCCR/PlanetS, Centre for Space and Habitability, University of Bern, Hochschulstrasse 4, 3012 Bern, Switzerland*
[15]*Department of Physics and Kavli Institute for Astrophysics and Space Research, Massachusetts Institute of Technology, Cambridge, MA 02139, USA*

Accepted 2022 March 16. Received 2022 March 16; in original form 2022 January 6

ABSTRACT

We are using precise radial velocities from CORALIE together with precision photometry from the Next Generation Transit Survey (NGTS) to follow-up stars with single-transit events detected with the Transiting Exoplanet Survey Satellite (*TESS*). As part of this survey, we identified a single transit on the star TIC-320687387, a bright ($T = 11.6$) G-dwarf observed by *TESS* in Sectors 13 and 27. From subsequent monitoring of TIC-320687387 with CORALIE, NGTS, and Lesedi we determined that the companion, TIC-320687387 B, is a very low-mass star with a mass of $96.2\pm^{1.9}_{2.0}\,M_{\rm J}$ and radius of $1.14\pm^{0.02}_{0.02}\,R_{\rm J}$ placing it close to the hydrogen burning limit ($\sim$80 $M_{\rm J}$). TIC-320687387 B is tidally decoupled and has an eccentric orbit, with a period of 29.77381 d and an eccentricity of 0.366 ± 0.003. Eclipsing systems such as TIC-320687387 AB allow us to test stellar evolution models for low-mass stars, which in turn are needed to calculate accurate masses and radii for exoplanets orbiting single low-mass stars. The sizeable orbital period of TIC-320687387 B makes it particularly valuable as its evolution can be assumed to be free from perturbations caused by tidal interactions with its G-type host star.

Key words: binaries: eclipsing.

1 INTRODUCTION

The small size and low luminosity of late M-dwarfs make them ideal targets to detect temperate terrestrial planets, such as those found in the TRAPPIST-1 system (Gillon et al. 2016, 2017). Planet occurrence rates for M-dwarf hosts from *Kepler* also appear to be higher than for FGK hosts (e.g. Hsu, Ford & Terrien 2020), and finding transiting planets around M-dwarfs is a key goal of the *TESS* mission (Ricker et al. 2015) as well as ground-based surveys such as MEarth (Nutzman & Charbonneau 2008) and SPECULOOS (Sebastian et al. 2021). *TESS* has already found 49 planets with M-dwarf host stars.[1]

★ E-mail: samuel.gill@warwick.ac.uk
† Winton Fellow.
‡ ESA Research Fellow.

[1]exoplanetarchive.ipac.caltech.edu - 2021-12-10

As with all transiting exoplanets, however, the planetary mass and radius can only be measured with respect to the properties of the host star. It is a concern therefore that observations of eclipsing M-dwarfs often reveal them to be cooler and larger than predicted by stellar models (e.g. Lubin et al. 2017; Parsons et al. 2018; and references therein). In order to accurately characterize the population of temperate exoplanets, it is therefore imperative that we understand these low-mass stars as completely as possible.

The tension between measured M-dwarf physical properties and models appears to span the spectral type with no obvious deviations around the transition from partially to fully convective stars (Parsons et al. 2018). Modification of stellar convection by magnetic fields is often invoked to explain these discrepancies (e.g. Chabrier, Gallardo & Baraffe 2007; Feiden & Chaboyer 2013a), with large star-spot fractions leading to cooler measured temperatures and radius inflation compensating for the lower flux from the photosphere. There have also been suggestions that the level of radius inflation is related to metallicity (e.g. Leggett et al. 2000; Berger et al. 2006; López-Morales 2007).

Much of the evidence for oversized M-dwarfs comes from eclipsing binary systems, where masses and radii can be measured precisely. These low-mass eclipsing binaries (EBLMs) have been found in large numbers with ground-based transit surveys such as WASP (Pollacco et al. 2006; Triaud et al. 2017; Gill et al. 2019). However, due to transit geometry, the known population of EBLMs is strongly weighted to short-period close binaries, where strong tidal interactions can maintain rapid rotation leading to enhanced magnetic activity (e.g. Kraus et al. 2011). This makes it difficult to separate single-star evolution from tidal effects experienced only in close binaries.

One way to find longer period tidally decoupled EBLMs is to exploit single-transit events detected with the *TESS* mission. We have begun a programme of photometric and spectroscopic follow-up of *TESS* single transit events, finding a mixture of long-period exoplanets (e.g. Gill et al. 2020c) and low-mass stellar companions (e.g. Gill et al. 2020a,b; Lendl et al. 2020; Grieves et al. 2021).

In this paper, we present the orbital solution of the *TESS* single-transit candidate TIC-320687387 AB, which we have found to be a G2 + M7 binary on a 30-d orbit. In Section 2, we describe the identification of the single-transit event as part of our warm Jupiter program, and we detail the observations required to measure the orbital solution. In Section 3, we describe our modelling of the TIC-320687387 AB system, while in Section 4 we discuss our results and the implications for radius inflation in late-type M-dwarfs.

2 OBSERVATIONS

2.1 *TESS* single-transit detection

We searched our own *TESS* full-frame light curves for single-transit events as described in Gill et al. (2020a,b,c). TIC-320687387 was observed with Camera 2 during Sectors 13 (2019-Jun-19 to 2019-Jul-18) and 27 (2020-Jul-04 to 2020-Jul-30). We identified a single transit event in our search of *TESS* Sector 13 data at JD 2458678.70408. TIC-320687387 A is a $T = 11.6$ G-dwarf, and we list its stellar parameters in Table 1. The transit depth was 11 ppt and is clearly significant compared with the out-of-transit light curve scatter of rms $= 0.1$ ppt (see Fig. 1). We carefully inspected calibrated *TESS* full-frame images for signs of asteroids, spacecraft jitter, stray light variations, or background eclipsing binaries. We found no evidence to suggest the event was anything other than a real astrophysical single-transit.

Table 1. Photometric colours, stellar atmospheric parameters, and physical properties of TIC-320687387 A.

Parameter	Value	Source
Gaia eDR3 source ID	6641131183310690432	1
RA	$19^{\rm h}51'18\farcs41$	1
Dec.	$-55°32'47''$	1
pmRA (mas yr^{-1})	31.827 ± 0.060	1
pmDec (mas yr^{-1})	-35.648 ± 0.048	1
Parallax (mas)	2.9720 ± 0.0351	1
Distance (pc)	336.5 ± 4.0	1
Magnitudes		
GAIA G	12.0148 ± 0.0002	1
GAIA BP	12.3383 ± 0.0012	1
GAIA RP	11.5246 ± 0.0009	1
TESS (T)	11.591 ± 0.006	2
APASS9 (B)	13.012 ± 0.398	3
APASS9 (V)	12.238 ± 0.028	3
2MASS (J)	10.955 ± 0.022	4
2MASS (H)	10.681 ± 0.026	4
2MASS (K_s)	10.624 ± 0.019	4
Spectroscopic parameters		
$T_{\rm eff}$ (K)	5780 ± 80	5
log g (dex)	4.4 ± 0.1	5
$\xi_{\rm t}$ (km s^{-1})	1.15 ± 0.18^6	5
$v_{\rm mac}$ (km s^{-1})	3.97 ± 0.73^6	5
V$\sin i$ (km s^{-1})	2.5 ± 0.8	5
[Fe/H] (dex)	0.30 ± 0.08	5
Host parameters		
$M_{\rm A}$ ($M_\odot$)	1.080 ± 0.034	5
$R_{\rm A}$ ($R_\odot$)	1.158 ± 0.016	5
Age (Gyr)	5 ± 3	5

Notes. [1]Gaia Collaboration et al. (2018), [2]Stassun et al. (2018), [3]Henden et al. (2015), [4]Skrutskie et al. (2006), [5]this work, [6]uncertainties from Doyle (2015).

TESS photometry of TIC-320687387 AB was also processed by the Science Processing Operations Center (SPOC; Jenkins et al. 2016) and made publicly available on the Mikulski Archive for Space Telescopes (MAST).[2] Measurements of Sector 13 was made at 30-min cadence and Sector 27 at 2-min cadence. We downloaded the *TESS* SPOC HLSP data (Caldwell et al. 2020) from MAST which included Simple Aperture Photometry (SAP) extracted from the pipeline-derived photometric aperture (Twicken et al. 2010; Morris et al. 2017) along with the Presearch Data Conditioning SAP (PDCSAP) light curve, which has been corrected for systematic trends shared by other stars on the detector (co-trending basis vectors). This product is significantly cleaner than its SAP counterpart and so we present the analysis of the SPOC HLSP PDCSAP light curve for Sector 13 at 30-min cadence and Sector 27 at 2-min cadence in this work (Fig. 1).

2.2 Spectroscopic follow-up with CORALIE

We made high-precision radial-velocity measurements of TIC-320687387 AB using CORALIE – a fiber-fed échelle spectrograph installed on the 1.2-m Leonard Euler telescope at the ESO La Silla Observatory (Queloz et al. 2001). A total of eight spectra were obtained between 2021 April 19 and July 20, each with an exposure time of 2400 s. The spectra were reduced using the standard CORALIE reduction pipeline, and radial velocity measurements

[2]https://mast.stsci.edu/

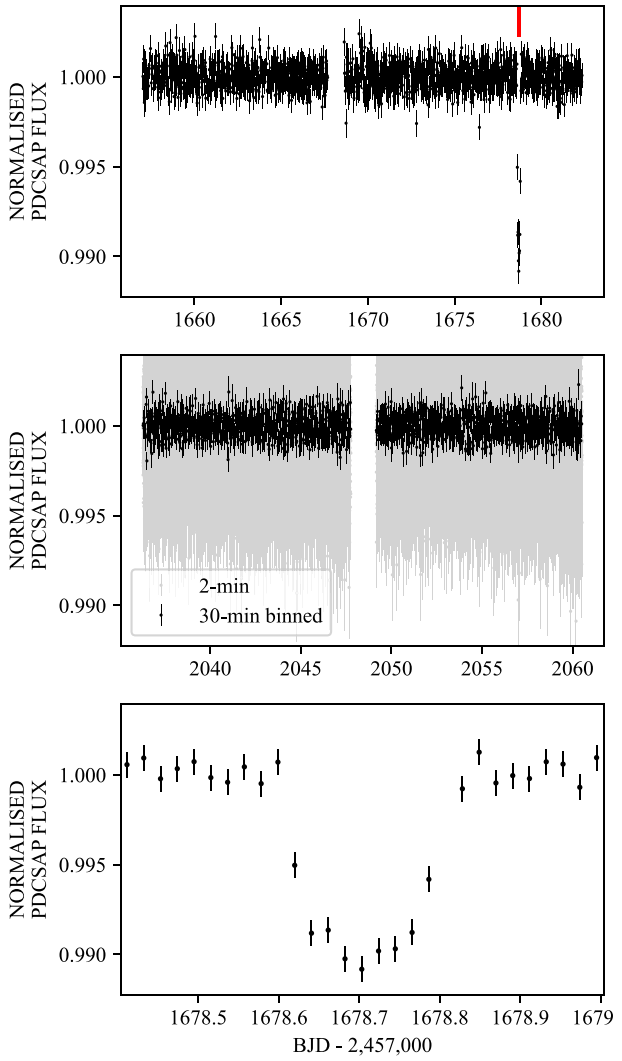

Figure 1. *TESS* SPOC light curves for Sector 13 (30-min cadence; upper panel) with the single transit event marked (red) along with Sector 27 (2-min cadence; middle panel). A closer look at the single-transit event in Sector 13 is shown in the lower panel.

Table 2. Radial velocity observations of TIC-320687387 AB and their associated errors from CORALIE.

JD	Radial velocity (km s^{-1})
2459323.873253	−50.0899 ± 0.0391
2459332.875484	−49.3755 ± 0.0486
2459345.853170	−55.0933 ± 0.0519
2459350.850859	−52.0922 ± 0.0851
2459363.842946	−52.7297 ± 0.0343
2459368.741216	−57.7449 ± 0.0300
2459375.766215	−54.9970 ± 0.0323
2459415.760069	−48.0367 ± 0.0448

derived from cross-correlation with a numerical G2 mask. These observations are summarized in Table 2 and plotted in Fig. 5 showing the best-fitting orbital solution. These data have a high radial velocity semi-amplitude consistent with a low-mass stellar companion on an eccentric orbit. We inspected potential dependencies between radial velocities and bisector spans and found little evidence of correlation.

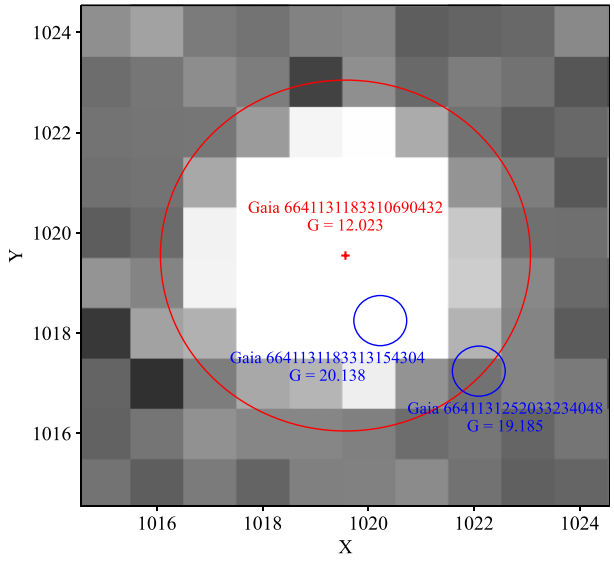

Figure 2. The NGTS reference image with the 3.5-pixel aperture plotted (red line) around TIC-320687387 AB (red cross) along with nearby stars from Gaia eDR3 (blue circles) with corresponding *Gaia* IDs and *Gaia G* magnitudes.

The radial velocity variations measured by CORALIE and the initial *TESS* transit were sufficient to determine the approximate orbital period of TIC-320687387 AB.

2.3 Transit photometry with NGTS

We also carried out photometric monitoring of TIC-320687387 AB from the night of 2021 May 8 using a single telescope of the Next generation Transit Survey (NGTS; Wheatley et al. 2018), which is located at the ESO Paranal Observatory in Chile. Each NGTS telescope has a field-of-view of 8 deg^2, providing sufficient reference stars for even the brightest TESS candidates. The telescopes have apertures of 20 cm and observe with a custom filter between 520–890 nm. We observed TIC-320687387 AB with 10-s exposures using a single telescope when the airmass was below 2.5 as part of a dedicated campaign to recover the orbital period TIC-320687387 AB. Data were reduced on-site the following day using standard aperture photometry routines. We used the template matching algorithm described in Gill et al. (2020a) to automatically search newly obtained NGTS photometric observations for transit events. In total, 121 738 photometric measurements of TIC-320687387 AB were made over 121 nights.

We detected two transit events on TIC-320687387 AB with NGTS. The first was an ingress event on the night of 2021 August 26 with a significance of $\Delta \log \mathcal{L} = 1244$, shown in the second panel of Fig. 5. The second transit event was on 2021 September 24 with $\Delta \log \mathcal{L} = 3355$, shown in the third panel of Fig. 5. This event constrains the transit width and impact parameter resulting in a more precise stellar density that otherwise possible with *TESS* alone. There are two faint sources that reside within the *Gaia* aperture (see Fig. 2). Both sources together contribute 0.192 per cent of the total flux in the aperture and cannot be the source of the transit events.

2.4 Transit photometry with Lesedi

The *TESS*, NGTS, and CORALIE observations were used to schedule a fourth transit event on 2021 October 24 using Lesedi, a new

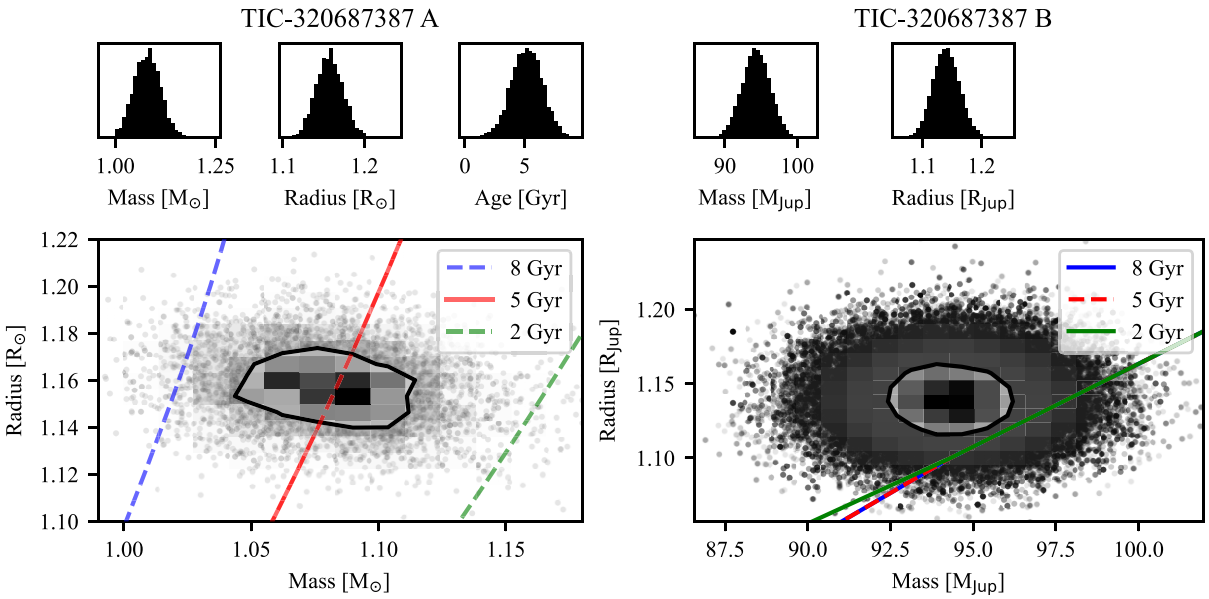

Figure 3. Upper panels show posterior probability distributions for mass, radius, and age of TIC-320687387 A (left-hand panels) and TIC-320687387 B (right-hand panels). Lower panels show 2D mass-radius posterior probability distributions with a 1σ contour (black line) along with isochrones for 2, 5, and 8 Gyr from MESA (TIC-320687387 A) and BHAC15 (TIC-320687387 B).

1-m telescope, at the South African Astronomical Observatory (SAAO). We obtained 1145 consecutive 8 s *V*-band images with the Sutherland High-speed Optical Camera, SHOC (Coppejans et al. 2013), a frame-transfer CCD camera with a 5.72 × 5.72 arcmin field of view (plate scale of 0.335 arcsec pix^{-1}), for a total observation time of 9160 s (2.54 h). Conditions during the observation were clear, with seeing improving from 2 to 1.5 arcsec, and ≈50 per cent humidity. The images were bias and flat-field corrected using the local PYTHON-based SHOC pipeline, which utilizes IRAF photometry tasks (PYRAF). We performed aperture photometry on the target and two comparison stars using the Starlink package AUTOPHOTOM. A 4-pixel radius aperture was selected to maximize the signal-to-noise ratio (S/N). The comparison stars were combined to perform differential photometry on the target. The resulting light curve is presented in Fig. 5.

3 ANALYSIS

3.1 Stellar atmospheric and physical parameters

We corrected each CORALIE spectrum into the laboratory reference frame using radial velocities from Table 2 and co-added them on to a common wavelength scale to create a high-quality spectrum with S/N ∼ 35. As described by Gill et al. (2020c), a grid of pre-computed model spectra were synthesized with the software package SPECTRUM (Gray 1999) using MARCS model atmospheres (Gustafsson et al. 2008), Version 5 of the GAIA ESO survey (GES) atomic line list and solar abundances from Asplund et al. (2009). Values of macroturbulence ($v_{\rm mac}$) and microturbulence ($\xi_{\rm t}$) were calculated using equations 5.10 and 3.1, respectively, from Doyle (2015). Given these models, we used the H α, NaI D, and MgI b lines to determine the stellar effective temperature, $T_{\rm eff}$, and surface gravity, log g. Individual Fe I and Fe II lines provided a measurement of metallicity, [Fe/H], and the rotational broadening projected into the line of sight, $V \sin i$.

We used the method described in Gill et al. (2020a) to determine the mass, radius, and age of TIC-320687387 A. This method uses *Gaia* magnitudes and parallax (Gaia Collaboration et al. 2018) along with $T_{\rm eff}$ and [Fe/H] from the spectroscopic analysis to determine the best-fitting stellar parameters with respect to MESA models (Choi et al. 2016; Dotter 2016). We found TIC-320687387 A to be a main-sequence G-type star. Our results are in good agreement with physical parameters predicted in Version 8 of the *TESS* input catalogue and the results of our analysis are shown in Fig. 3 and presented in Table 1.

3.2 Orbital geometry and transit properties

We modelled all photometric and radial velocity data sets simultaneously. As part of the SPOC pipeline, the PDCSAP light curve has been corrected for assuming a contamination ratio of 3.668 per cent (calculated from Version 8 of the *TESS* input catalogue; Stassun et al. 2018). From initial modelling, we found this to be an under correction. We argue this likely originates from a catalogue error which underpredicts the contamination ratio for TIC-320687387; such issues affect ∼ 1 per cent of *TESS* SPOC target stars.[3] Additionally, we find that a tertiary companion of different colour is unlikely as the deeper NGTS transits are observed through a similar filter and have consistent transit depths with the bluer Lesedi observations. To account for this, we fit an additional dilution term, $l_{3,\rm TESS}$, to the PDCSAP light curve. We used the binary star model described by Gill et al. (2020a) to calculate models of radial velocity and transit photometry. This utilizes the analytical transit model for the power-2 limb-darkening law presented by Maxted & Gill (2019). We fit decorrelated limb-darkening parameters h_1 and h_2 (from equations 1 and 2 of Maxted 2018) with Gaussian priors centred on values interpolated from table 2 of Maxted (2018) using stellar atmospheric parameters from Table 1 and widths of 0.003 and 0.046, respectively. The subtle differences between *TESS*, NGTS, and Lesedi's *V*-band

[3]Private communication.

Table 3. Orbital solution of the TIC-320687387 AB system. Asymmetric errors are reported in brackets and correspond to the difference between the median and the 16th (lower value) and 84th (upper value) percentile.

Parameter	Value
Fitted parameters	
T_0 (JD)	$2459452.82405^{(98)}_{(98)}$
Period (d)	$29.77381^{(12)}_{(12)}$
R_A/a	$0.0289^{(13)}_{(15)}$
R_B/R_A	$0.1012^{(18)}_{(14)}$
b	$0.639^{(176)}_{(144)}$
$h_{1,TESS}$	$0.7873^{(23)}_{(22)}$
$h_{2,TESS}$	$0.4405^{(357)}_{(350)}$
$h_{1,NGTS}$	$0.7638^{(23)}_{(23)}$
$h_{2,NGTS}$	$0.4580^{(360)}_{(350)}$
$h_{1,Lesedi}$	$0.7044^{(24)}_{(24)}$
$h_{2,Lesedi}$	$0.4681^{(365)}_{(364)}$
zp_{TESS}	$1.00013^{(20)}_{(19)}$
zp_{NGTS}	$0.99990^{(12)}_{(13)}$
zp_{Lesedi}	$0.99976^{(14)}_{(14)}$
$l_{3,TESS}$	$0.110^{(52)}_{(50)}$
σ_{TESS}	$0.00014^{(9)}_{(13)}$
σ_{NGTS}	$0.00047^{(24)}_{(21)}$
σ_{Lesedi}	$0.00441^{(8)}_{(8)}$
K_A (km s^{-1})	$5.983^{(27)}_{(26)}$
f_s	$0.563^{(3)}_{(3)}$
f_c	$0.220^{(4)}_{(4)}$
V_0 (km s^{-1})	$-52.576^{(13)}_{(12)}$
J (km s^{-1})	$0.016^{(11)}_{(8)}$

transmission filters are such that we fitted independent values of h_1 and h_2 for each photometric data set. The orbital period and eccentricity yield a light traveltime on the order of 1–2 min which is significant for the cadence of NGTS and Lesedi observations; our model accounts for light traveltime delays which causes the transits to appear early. Preliminary modelling yielded consistent transit depths across different colours and so we decide to fit a common value of $k = R_B/R_A$. The luminosity ratio between the host and transiting companion are such that we do not expect to see a secondary eclipse or significant dilution of the primary eclipse in our data sets (see Section 4.6).

Our model vector included the transit epoch (T_0), the orbital period (P), the scaled orbital separation (R_A/a), the ratio of radii ($k = R_B/R_A$), the impact parameter (b), $l_{3,TESS}$, independent values of the photometric zero-point (zp), h_1 and h_2 for each photometric data set, the radial-velocity semi-amplitude (K_A), and the systematic radial velocity of the primary star (V_0). We avoid fitting the strongly correlated eccentricity (e) and the argument of the periastron (ω) and instead used $f_c = \sqrt{e}\cos\omega$ and $f_s = \sqrt{e}\sin\omega$ since these are less correlated and have more uniform prior probability distributions. CORALIE radial velocity errors are occasionally underestimated in-part due to spot activity, pulsations, and granulation which can introduce noise in to the radial velocity measurements (Ford 2006). To mitigate this, we include a jitter term, J, which is added in quadrature with CORALIE radial velocity errors. We fit a similar term for each photometric data set, σ, which was also added in quadrature to photometric uncertainties.

Table 4. Derived and physical properties of the TIC-320687387 AB system. Asymmetric errors are reported in brackets and correspond to the difference between the median and the 16th (lower value) and 84th (upper value) percentile.

Parameter	Value
width (hr)	$5.87\pm^{0.38}_{0.52}$
ρ_A ($\rho_\odot$)	$1.73\pm^{0.25}_{0.24}$
log g_B (dex)	$5.20\pm^{0.05}_{0.06}$
M_B ($M_\odot$)	$0.0900\pm^{0.0018}_{0.0019}$
M_B (M_J)	$96.2\pm^{1.9}_{2.0}$
R_B ($R_\odot$)	$0.1171\pm^{0.0024}_{0.0023}$
R_B (R_J)	$1.14\pm^{0.02}_{0.02}$
e	$0.366\pm^{0.003}_{0.003}$
ω ($^\circ$)	$68\pm^{41}_{40}$
a periastron (au)	$0.118\pm^{0.006}_{0.006}$
a apastron (au)	$0.255\pm^{0.012}_{0.013}$

The Bayesian sampler EMCEE (Foreman-Mackey et al. 2013) was used to explore parameter space and determine the best-fitting model for the TIC-320687387 AB system. We drew 100 000 steps from 46 Markov chains and discarded the first 50 000 steps as part of the burn-in phase. After visually confirming each chain had converged, we selected the trial step with the highest log-likelihood was chosen as our measurement for each fitted parameter. Asymmetric uncertainties were calculated from the difference between each measured parameter and the 16th and 84th percentiles of their cumulative posterior probability distributions.

For each valid trial step, we calculate the transit width using equation (3) from Seager & Mallén-Ornelas (2003). We draw random values of M_A and R_A from a normal distribution centred on measured values from Table 1 with width equal to their respective uncertainties. These were combined with trial values of P, e, and K_A to make a closed-form solution of the cubic polynomial required to solve the mass function

$$\frac{(M_B \sin i)^3}{(M_A + M_B)^2} = (1 - e^2)^{\frac{3}{2}} \frac{P K_A^3}{2\pi G}, \quad (1)$$

for M_B. The mass ratio, $q = M_B/M_A$, can then be used with R_A/a, f_s, and f_c to estimate the stellar density using equations (1) and (2) from Van Eylen & Albrecht (2015) along with surface gravity of the transiting companion using equation (4) from Southworth, Wheatley & Sams (2007). Trial values of R_A and k were combined to calculate R_B. The measured values from our joint analysis are summarized in Table 3 and Fig. 5 along with derived parameters shown in Table 4.

3.3 Star-spot modulation

Independent measurements of the rotation period came from NGTS photometry which show a subtle brightening/dimming effect as star-spots come in and go from the facing hemisphere of TIC-320687387 A. The longevity of spots is a limiting factor for measuring the rotational period and we assume that the average spot lifetime exceeds the rotation period of TIC-320687387 A. A Lomb-–Scargle analysis of the out-of-transit NGTS photometry for TIC-320687387 reveals a significant (sde > 8) peak at 22.53 d (Fig. 4) corresponding

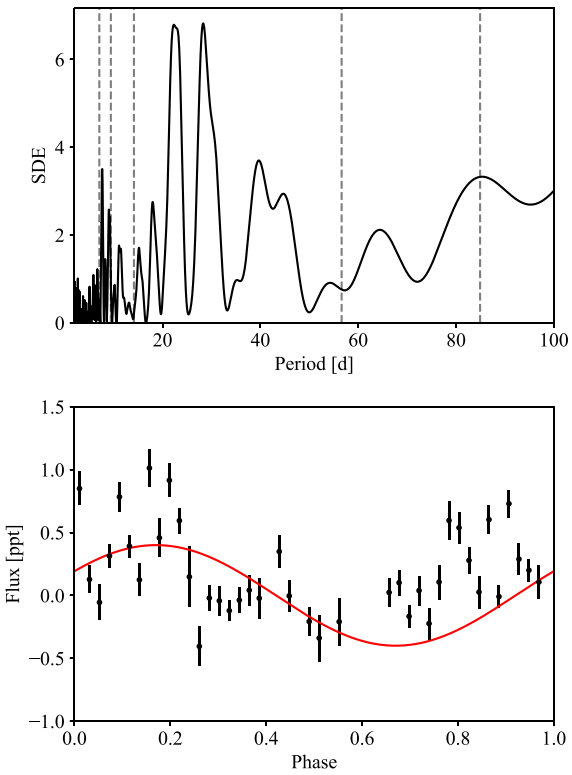

Figure 4. Upper panel: Lomb–Scargle diagram for the out of transit NGTS photometery (black) with peaks marking harmonics (grey vertical lines). The peak of the Lomb–Scargle periodogram (22.53-d period) is marked with a black arrow. Lower panel: phased and binned NGTS photometry on the 22.53-d period with the best-fitting sinusoid (red) indicating a 0.4 ppt modulation likely caused by star-spots and stellar rotation.

to 0.4 ppt variation equivalent to a rigid body rotational velocity of $\sim 2.6\,\mathrm{km\,s^{-1}}$.

4 DISCUSSION

4.1 The TIC-320687387 AB system

Spectral analysis reveals that TIC-320687387 A is richer in metals than the Sun and has spectral type G2V. Gravity-sensitive Mg III and Na II lines appear consistent with a star on the main sequence. The transiting companion is a low-mass star with an estimated spectral type M7 based on mass and radius measurements. It is expected to be fully convective and we assume any magnetic field will be sustained with a mechanism like the α^2-dynamo (Chabrier & Küker 2006). The M-dwarf is close to the best-fitting isochrone (Fig. 5) compared to similarly measured objects but we do find a marginally significant inflation (1.8σ). In the following sections, we discuss interesting aspects of the TIC-320687387 AB system.

4.2 Possible inflation of the M-dwarf companion

In Fig. 6, we show the mass and radius of TIC-320687387 B amongst recently measured eclipsing brown dwarfs and late M-dwarfs. TIC-320687387 B is relatively close to stellar models but its measured inflation is marginally significant (1.8σ). We assume a coeval formation of the TIC-320687387 AB system around 5 ± 3 Gyr

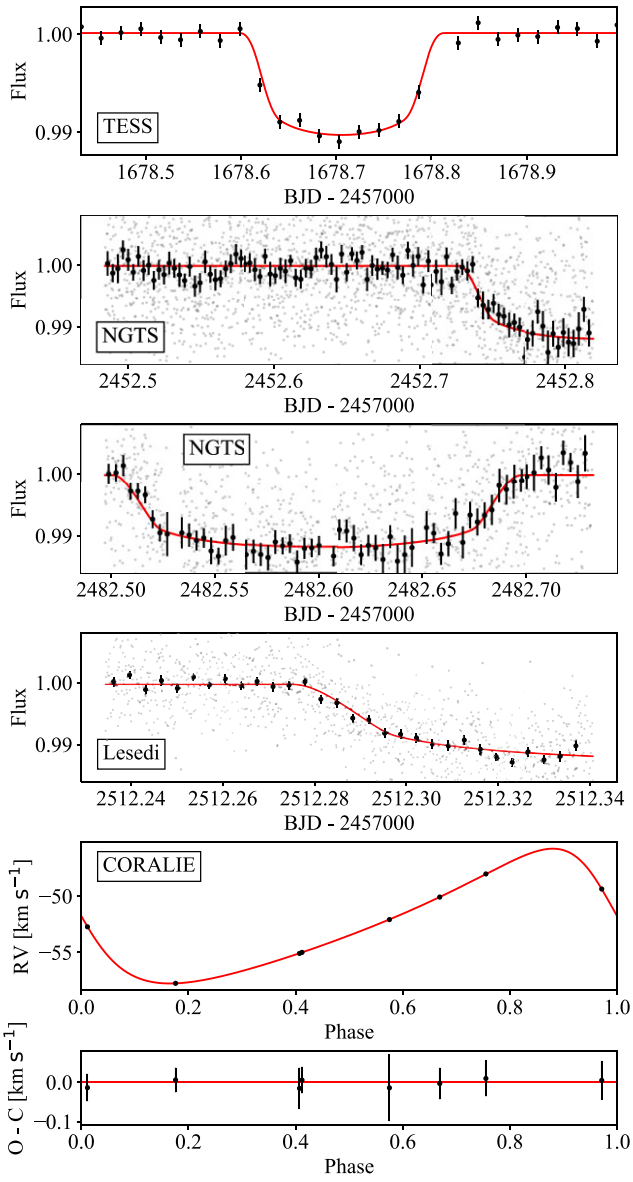

Figure 5. Orbital solution for TIC-320687387 AB. Transit photometry (black) is shown *TESS* (upper panel), NGTS (upper middle panels), and Lesedi (low middle panel) with the best-fitting models (red). For NGTS and Lesedi, we show the 5-min binned light curve. Lower middle panel: CORALIE radial velocity measurements (black) with the best-fitting model (red); Lower panel: fit residuals.

ago. The mass of TIC-320687387 B is where 2–8 Gyr stellar models show little difference in predicted radii and so age has little bearing on measured inflation.

The measured inflation may be statistical but there is a possibility it is indeed real. Measuring the radius of TIC-320687387 B is dependent on stellar models used to measure the physical properties of TIC-320687387 A. These in-turn depend on critical input values of a mixing length parameter and helium enhancement. Gill et al. (2019) used five EBLM systems to measure an additional 3–5 per cent uncertainty in the mass of the host star when accounting for uncertainties in mixing length parameter and helium enhancement. The sample used by Gill et al. (2019) consisted of hotter F-type stars and were compared to models from the GARSTEC stellar evolution code (Weiss & Schlattl 2008). Nevertheless a 3.7- per cent increase

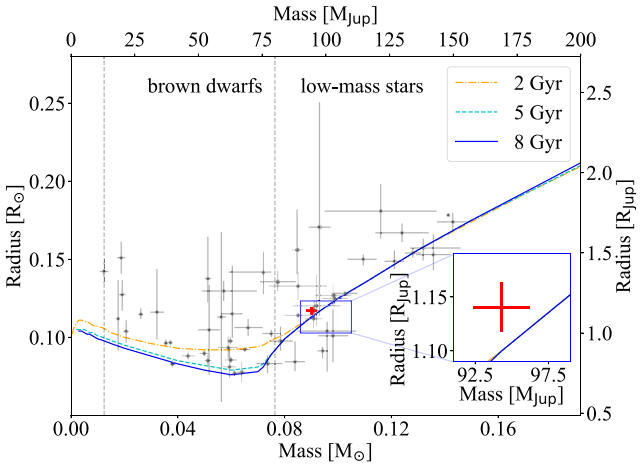

Figure 6. Mass–radius diagram for 54 brown dwarfs and low-mass stars (black) presented in Grieves et al. (2021). Gray vertical lines mark the approximate locations of the planet/brown dwarf boundary ($\sim 13\,M_{Jup}$) and the brown dwarf/M-dwarf boundary ($\sim 80\,M_{Jup}$). We show the 5-Gyr isochrone (cyan) from Baraffe et al. (2002, 2015) and mark TIC-320687387 B in red. An inset axis highlights TIC-320687387 B with respect to the best-fitting isochrone.

in mass would mean TIC-320687387 B was consistent with stellar models.

In contrast to the mass and radius, the surface gravity of TIC-320687387 B is determined entirely from fitted parameters. We find the value $\log g_B = 5.20^{(5)}_{(6)}$ dex is slightly below the expected value of 5.29 dex from the 5 Gyr isochrone. This result provides evidence for modest inflation independent of models for TIC-320687387 A, although we note that these values are still consistent within 2σ.

We are confident that TIC-320687387 B does not exhibit an enhanced dynamo due to tidal interaction, but it may still be significantly spotted. The luminosity ratio between the two components ($\sim 10^{-4}$) is such that we are unable to detect photometric modulation from TIC-320687387 B but it may have a non-negligible spot coverage which could account for the small measured inflation (López-Morales & Ribas 2005; Feiden & Chaboyer 2013b).

4.3 The hydrogen burning limit

Brown dwarfs are sub-stellar objects residing between giant planets ($\sim 13\,M_J$) and low-mass main-sequence stars ($\sim 80\,M_J$), with the upper boundary defined by the mass required for stable thermonuclear fusion of hydrogen. During their first few million years, both M dwarfs and brown dwarfs produce energy by fusing deuterium, with their cores contracting and heating up. Fusion of hydrogen via the proton–proton chain requires a sufficiently high pressure that brown dwarfs never reach due in-part to their core density providing a sufficient restoring force with electron degeneracy pressure. Ultimately, M-dwarfs go on to fuse hydrogen for billions of years (Baraffe et al. 1998) compared to brown dwarfs that exhaust their comparatively sparse deuterium supply in a few million years before cooling and shrinking (Spiegel, Burrows & Milsom 2011).

The exact transition between brown dwarfs and M dwarfs depends on a number of initial formation conditions including the size of the initial protostar, metal and deuterium abundances, stellar opacity, and the convective efficiency of the outer layers (Chabrier & Baraffe 1997; Baraffe et al. 2002). The generally adopted boundary is $\sim 80\,M_J$ (e.g. Marcy & Butler 2000; Grether & Lineweaver 2006) which is a median between an array of model predictions spanning 73.3–96.4 M_J (see Dieterich et al. 2018, and references therein). TIC-320687387 B is near the top of this range ($96.2 \pm 0.2\ M_J$) suggesting that it could reside within the brown dwarf transition. However, its consistency with the 5-Gyr isochrone suggests it is indeed stellar in nature.

4.4 Rotational modulation

The measured rotation period from NGTS photometry ($P_{rot} = 22.53$ d) corresponds to a surface rotation of $\sim 2.6\,km\,s^{-1}$ which is consistent the spectroscopic value of $V \sin i = 2.5 \pm 0.8\,km\,s^{-1}$. This suggests that the rotation axis is broadly aligned with the orbital axis. We expected mutual stellar and orbital inclinations but past dynamical interactions may have misaligned the two. This can be confirmed with future measurements of the Rossiter–McLaughlin effect for the TIC-320687387 AB system.

4.5 Orbital dynamics

The great advantage of systems like TIC-320687387 AB is that they are tidally decoupled. M-dwarfs characterized in these systems are therefore more akin to isolated field M-dwarfs and can be more robustly compared to stellar models. The significant eccentricity of the TIC-320687387 AB system results in an orbital separation of 0.255 au at apastron and 0.118 au at periastron. For long period binaries like TIC-320687387 AB, we expect tidal circularization to be exceptionally weak when accounting for the binary mass ratio, q. Work by Claret & Cunha (1997) determined a semi-empirical calibration joining the physical parameters of the binary system with critical circularization and synchronization time-scales for those with convective and radiative envelopes (see their equations 15–18). These relations suggest τ_{circ} is many times greater than the age of the TIC-320687387 AB system and has played a negligible role in any orbital evolution. Additionally, it is possible for a tertiary companion to excite the eccentricity to larger values despite a low primordial eccentricity (Mazeh & Shaham 1979). We find no evidence of a stellar tertiary companion in either the photometric (transit timing variations) or spectroscopic (radial velocity residuals) data sets and find this scenario unlikely for the TIC-320687387 AB system. It is possible that efficiency of tidal circularization may have been larger during the pre-main-sequence phase when the host star would have been much larger (Zahn 1989; Zahn & Bouchet 1989). However, this increase would have been marginal given the orbital separation and the expected radii of both stars during the pre-main-sequence.

It is of interest to understand the rotation and stellar inclination of TIC-320687387 A. One could argue for mutual stellar and orbital inclination as they are relics of the angular momentum from a common primordial cloud. However, their large orbital separation could have resulted in quasi-local formation and dynamical interactions which may not have preserved the alignment between rotation and orbital inclinations. If the latter is the case, the time-scale of aligning the orbital and spin axis is on the same order as tidal synchronization which far exceeds the lifetime of this system (Claret & Cunha 1997). We calculated the posterior probability distribution for the inclination of TIC-320687387 A's spin axis relative to the line of sight (Fig. 7) using a Monte Carlo technique and correct analytical expression from Masuda & Winn (2020) given the measured value of V sin i from Table 1 and rotational velocity from Section 3.3 with an assumed 5-per cent uncertainty. The analytical expression peaks at an inclination of 73.°65 suggesting a spin-orbit misalignment of $\sim 16^\circ$. However, the posterior probability distribution is almost constant

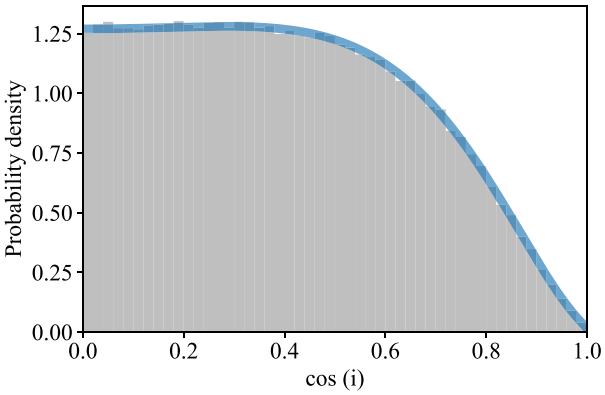

Figure 7. Monte Carlo probability distribution for the inclination of the TIC-320687387 A's spin axis relative to the line of sight (grey) with the correct analytical expression (blue) from Masuda & Winn (2020).

between rotational inclinations 60°–90° before tailing off for lower inclinations. This suggests that spin-orbit misalignments between ∼0–30° are equally probable for the TIC-320687387 AB system with a higher obliquity less likely. Four systems within the EBLM project include measurements of spin-orbit misalignment: WASP-30 and EBLM J1219–39 (Triaud et al. 2013), EBLM J0218–31 (Gill et al. 2019), and EBLM J0608–59/TOI-1338 (Kunovac Hodžić et al. 2020) with all suggesting coplanar stellar rotation and orbital axes. The orbital periods of these systems are shorter than TIC-320687387 AB and more likely to be affected by tides. Therefore, it would be of interest to measure the spin-orbit misalignment for TIC-320687387 AB and see if it is consistent with those of shorter orbital periods.

4.6 Secondary eclipse

The orbital dynamics of TIC-320687387 AB indicates a secondary eclipse centred at phase 0.705 (0.7025–0.7075) which both *TESS* and NGTS data sets cover. We calculate the expected secondary eclipse depth by interpolating PHOENIX model spectra (Husser et al. 2013) for the each component in the TIC-320687387 AB system. For TIC-320687387 A, we use values of $T_{\rm eff}$ and log g from Table 1. For TIC-320687387 B, we use log $g_{\rm B}$ from Table 4 and use empirical calibrations[4] to estimate $T_{\rm effB} = 2680$ K. Transmission filters[5] for NGTS and *TESS* were used to calculate a secondary eclipse depth of 108 and 267 ppm, respectively. This is significantly below the noise profile of both *TESS* and NGTS data sets and we do not claim any detection of a secondary eclipse. This will be significantly deeper in the infrared where the luminosity ration between TIC-320687387 A and B becomes less extreme. For 2MASS filters J, H, and $K_{\rm s}$, we calculate secondary eclipse depths of 1.1, 1.4, and 1.9 ppt, respectively. This is within the capabilities of modern ground-based infrared telescopes and would provide a measurement of the stellar effective temperature for TIC-320687387 B. EBLM systems with measured secondary eclipses have revealed M-dwarfs with effective temperatures in excess of predicted by stellar models (e.g. J0113+31; Gómez Maqueo Chew et al. 2014) and it would be of interest to see if TIC-320687387 B is similar.

[4]www.pas.rochester.edu/ emamajek/EEM_dwarf_UBVIJHK_colors_Teff.txt; accessed 2021 Dec 29
[5]from svo2.cab.inta-csic.es; accessed 2021 Dec 29

5 CONCLUSION

TIC-320687387 AB is a long-period EBLM system with a very low-mass secondary star close to the hydrogen burning limit. Tidal effects on both components are negligible due to a substantial orbital separation.

The low-mass companion TIC-320687387 B was initially identified through a single-transit event in *TESS* full-frame light curves from Sector 13. The transit depth and width were consistent with a Jovian planet and so we commenced a ground-based spectroscopic and photometric campaign to recover the orbital period. A total of eight CORALIE radial velocities (Table 2) first provided an approximate spectroscopic orbit followed by two transits with NGTS and one transit with Lesedi which confirmed an orbital period of 29.77381 d. Spectroscopic observations were used to measure physical and stellar atmospheric parameters of TIC-320687387 A. They confirmed a spectral type G2 with mass, temperature, radius, and age similar to the Sun (Table 1 and Fig. 3).

Joint analysis of photometric and spectroscopic data sets (Fig. 5, Tables 3 and 4) revealed TIC-320687387 B to be a late M-dwarf ($M_{\rm B} = 96.2\pm^{1.9}_{2.0}\,M_{\rm J}$, $R_{\rm B} = 1.14\pm^{0.02}_{0.02}\,R_{\rm J}$) near the hydrogen burning limit (∼80 $M_{\rm J}$). The mass and radius of TIC-320687387 B is closer to stellar models than many other M-dwarfs from the literature (mostly in much closer binaries). However, we do find a marginally significant inflation (1.8σ) which might be statistical or may be a real offset. We measure a moderately high eccentricity of the TIC-320687387 AB system ($e = 0.366 \pm 0.003$) which likely remains from formation due to a large orbital separation diminishing any tidal influence between components. With NGTS, we measure a likely spot modulation indicating a rotational period of 22.53 d which is consistent with the projected rotation measured from spectroscopic analysis.

Most EBLMs with precise measurements of physical parameters have orbital periods below ∼ 10 d and are subjected to tidal interactions which complicate discussions of systematic inflation. Longer period systems tend to be free of this and are more akin to field M-dwarfs, which are the subject of intense surveys for small transiting exoplanets by *TESS* and other instruments. An increasing number of precisely measured systems like TIC-320687387 AB will allow us to test models of stellar evolution for the smallest main-sequence stars and better understand the planets we find around them.

ACKNOWLEDGEMENTS

The NGTS facility is operated by the consortium institutes with support from the UK Science and Technology Facilities Council (STFC) under projects ST/M001962/1 and ST/S002642/1. We acknowledge the use of public *TESS* data from pipelines at the TESS Science Office and at the TESS Science Processing Operations Centre. This paper includes data collected with the TESS mission, obtained from the MAST data archive at the Space Telescope Science Institute (STScI). Funding for the TESS mission is provided by the NASA Explorer Program. STScI is operated by the Association of Universities for Research in Astronomy, Inc., under NASA contract NAS 5-26555. Based on observations made with ESO Telescopes at the La Silla Paranal Observatory under programme IDs 0104.*C* − 0413 (PI RB), 0104.*C* − 0588 (PI FB), Opticon:2019A/037 (PI DB), and CNTAC: 0104.*A* − 9012 (PI JIV). This paper uses observations made at the SAAO. The contributions at the University of Warwick by PJW, RGW, DRA, and SG have been supported by STFC through consolidated grants ST/L000733/1 and ST/P000495/1. Contributions at the University of Geneva by SUl, NG, ML, FB, LM, and SUd

were carried out within the framework of the National Centre for Competence in Research 'PlanetS' supported by the Swiss National Science Foundation (SNSF). ML acknowledges support of the Swiss National Science Foundation under grant number PCEFP2194576. This research has made use of NASA's Astrophysics Data System Bibliographic Services and the SIMBAD data base, operated at CDS, Strasbourg, France. This research made use of ASTROPY,[6] a community-developed core PYTHON package for Astronomy (Astropy Collaboration et al. 2018). MNG acknowledges support from the European Space Agency (ESA) as an ESA Research Fellow. JSJ acknowledges support by FONDECYT grant 1201371 and partial support from the ANID Basal project FB210003. The work of HPO has been carried out within the framework of the NCCR PlanetS supported by the Swiss National Science Foundation. EG gratefully acknowledges support from the David and Claudia Harding Foundation in the form of a Winton Exoplanet Fellowship.

DATA AVAILABILITY

The *TESS* SPOC data for TIC-320687387 is publicly available on the MAST. Reduced CORALIE spectra, derived measurements of radial velocities, and full photometric data sets from NGTS and Lesedi will be available from the VizieR archive server hosted by the Université de Strasbourg.[7]

REFERENCES

Asplund M., Grevesse N., Sauval A. J., Scott P., 2009, ARA&A, 47, 481
Astropy Collaboration et al., 2018, AJ, 156, 123
Baraffe I., Chabrier G., Allard F., Hauschildt P. H., 1998, A&A, 337, 403
Baraffe I., Chabrier G., Allard F., Hauschildt P. H., 2002, A&A, 382, 563
Baraffe I., Homeier D., Allard F., Chabrier G., 2015, A&A, 577, A42
Berger D. H. et al., 2006, ApJ, 644, 475
Caldwell D. A. et al., 2020, Res. Not. Am. Astron. Soc., 4, 201
Chabrier G., Baraffe I., 1997, A&A, 327, 1039
Chabrier G., Gallardo J., Baraffe I., 2007, A&A, 472, L17
Chabrier G., Küker M., 2006, A&A, 446, 1027
Choi J., Dotter A., Conroy C., Cantiello M., Paxton B., Johnson B. D., 2016, ApJ, 823, 102
Claret A., Cunha N. C. S., 1997, A&A, 318, 187
Coppejans R. et al., 2013, PASP, 125, 976
Dieterich S., Henry T., Jao W. C., Washington R., Silverstein M., Winters J., RECONS, 2018, AAS Meeting Abstracts,#349.18
Dotter A., 2016, ApJS, 222, 8
Doyle A. P., 2015, PhD thesis, Keele Univ.
Feiden G. A., Chaboyer B., 2013a, EAS Publ. Ser., 64 127
Feiden G. A., Chaboyer B., 2013b, ApJ, 779, 183
Ford E. B., 2006, ApJ, 642, 505
Foreman-Mackey D., Hogg D. W., Lang D., Goodman J., 2013, PASP, 125, 306
Gaia Collaboration et al., 2018, A&A, 616, A1
Gill S. et al., 2019, A&A, 626, A119
Gill S. et al., 2020a, MNRAS, 491, 1548
Gill S. et al., 2020b, MNRAS, 495, 2713
Gill S. et al., 2020c, ApJ, 898, L11
Gillon M. et al., 2016, Nature, 533, 221
Gillon M. et al., 2017, Nature, 542, 456
Gómez Maqueo Chew Y. et al., 2014, A&A, 572, A50
Gray R. O., 1999, Astrophysics Source Code Library, record ascl: 9910.002
Grether D., Lineweaver C. H., 2006, ApJ, 640, 1051
Grieves N. et al., 2021, A&A, 652, A127
Gustafsson B., Edvardsson B., Eriksson K., Jørgensen U. G., Nordlund Å.,Plez B., 2008, A&A, 486, 951
Henden A. A., Levine S., Terrell D., Welch D. L., 2015, AAS Meeting Abstracts, #336.16
Hsu D. C., Ford E. B., Terrien R., 2020, MNRAS, 498, 2249
Husser T. O., Wende-von Berg S., Dreizler S., Homeier D., Reiners A., Barman T., Hauschildt P. H., 2013, A&A, 553, A6
Jenkins J. M. et al., 2016, in Chiozzi G., Guzman J. C., eds, SPIE Conf. Ser., Vol. 9913, Software and Cyberinfrastructure for Astronomy IV. SPIE, Bellingham, p. 99133E
Kraus A. L., Tucker R. A., Thompson M. I., Craine E. R., Hillenbrand L. A., 2011, ApJ, 728, 48
Kunovac Hodžić V. et al., 2020, MNRAS, 497, 1627
Leggett S. K., Allard F., Dahn C., Hauschildt P. H., Kerr T. H., Rayner J., 2000, ApJ, 535, 965
Lendl M. et al., 2020, MNRAS, 492, 1761
López-Morales M., 2007, ApJ, 660, 732
López-Morales M., Ribas I., 2005, ApJ, 631, 1120
Lubin J. B. et al., 2017, ApJ, 844, 134
Marcy G. W., Butler R. P., 2000, PASP, 112, 137
Masuda K., Winn J. N., 2020, AJ, 159, 81
Maxted P. F. L., 2018, A&A, 616, A39
Maxted P. F. L., Gill S., 2019, A&A, 622, A33
Mazeh T., Shaham J., 1979, A&A, 77, 145
Morris R. L., Twicken J. D., Smith J. C., Clarke B. D., Jenkins J. M., Bryson S. T., Girouard F., Klaus T. C., 2017, Kepler Data Processing Handbook: Photometric Analysis. Kepler Science Document KSCI-19081-002. NASA Ames Research Center
Nutzman P., Charbonneau D., 2008, PASP, 120, 317
Parsons S. G. et al., 2018, MNRAS, 481, 1083
Pollacco D. L. et al., 2006, PASP, 118, 1407
Queloz D. et al., 2001, A&A, 379, 279
Ricker G. R. et al., 2015, J. Astron. Teles. Instrum. Syst., 1, 014003
Seager S., Mallén-Ornelas G., 2003, ApJ, 585, 1038
Sebastian D. et al., 2021, A&A, 645, A100
Skrutskie M. F. et al., 2006, AJ, 131, 1163
Southworth J., Wheatley P. J., Sams G., 2007, MNRAS, 379, L11
Spiegel D. S., Burrows A., Milsom J. A., 2011, ApJ, 727, 57
Stassun K. G. et al., 2018, AJ, 156, 102
Triaud A. H. M. J. et al., 2013, A&A, 549, A18
Triaud A. H. M. J. et al., 2017, A&A, 608, A129
Twicken J. D., Clarke B. D., Bryson S. T., Tenenbaum P., Wu H., Jenkins J. M., Girouard F., Klaus T. C., 2010, in Radziwill N. M., Bridger A., eds, SPIE Conf. Ser., Vol. 7740, Software and Cyberinfrastructure for Astronomy. SPIE, Bellingham, p. 774023
Van Eylen V., Albrecht S., 2015, ApJ, 808, 126
Weiss A., Schlattl H., 2008, Ap&SS, 316, 99
Wheatley P. J. et al., 2018, MNRAS, 475, 4476
Zahn J. P., 1989, A&A, 220, 112
Zahn J. P., Bouchet L., 1989, A&A, 223, 112

[6] www.astropy.org
[7] cdsarc.u-strasbg.fr

This paper has been typeset from a TEX/LATEX file prepared by the author.